Electromagnetic Moments of Radioactive ^{136}Te and the Emergence of Collectivity 2p ⊕ 2n Outside of Double-Magic ^{132}Sn

J. M. Allmond,[1] A. E. Stuchbery,[2] C. Baktash,[1] A. Gargano,[3] A. Galindo-Uribarri,[1,4] D. C. Radford,[1] C. R. Bingham,[1,4] B. A. Brown,[5,6] L. Coraggio,[3] A. Covello,[7] M. Danchev,[4,8] C. J. Gross,[1] P. A. Hausladen,[9] N. Itaco,[3,10] K. Lagergren,[9] E. Padilla-Rodal,[11] J. Pavan,[9] M. A. Riley,[12] N. J. Stone,[4,13] D. W. Stracener,[1] R. L. Varner,[1] and C.-H. Yu[1]

[1]*Physics Division, Oak Ridge National Laboratory, Oak Ridge, Tennessee 37831, USA*
[2]*Department of Nuclear Physics, Australian National University, Canberra ACT 0200, Australia*
[3]*Istituto Nazionale di Fisica Nucleare, Complesso Universitario di Monte S. Angelo, Via Cintia, I-80126 Napoli, Italy*
[4]*Department of Physics and Astronomy, University of Tennessee, Knoxville, Tennessee 37996, USA*
[5]*National Superconducting Cyclotron Laboratory, Michigan State University, East Lansing, Michigan 48824, USA*
[6]*Department of Physics and Astronomy, Michigan State University, East Lansing, Michigan 48824, USA*
[7]*Dipartimento di Fisica "Ettore Pancini", Università di Napoli Federico II, Complesso Universitario di Monte S. Angelo, Via Cintia, I-80126 Napoli, Italy*
[8]*Faculty of Physics, St. Kliment Ohridski University of Sofia, 1164 Sofia, Bulgaria*
[9]*Joint Institute for Heavy Ion Research, Oak Ridge National Laboratory, Oak Ridge, Tennessee 37831, USA*
[10]*Dipartimento di Matematica e Fisica, Università degli Studi della Campania "Luigi Vanvitelli", Viale Abramo Lincoln 5, I-81100 Caserta, Italy*
[11]*Instituto de Ciencias Nucleares, UNAM, AP 70-543, 04510 Mexico City, Mexico*
[12]*Department of Physics, Florida State University, Tallahassee, Florida 32306, USA*
[13]*Department of Physics, Oxford University, Oxford, OX1 3PU, United Kingdom*

(Received 5 December 2016; published 3 March 2017)

Radioactive ^{136}Te has two valence protons and two valence neutrons outside of the ^{132}Sn double shell closure, providing a simple laboratory for exploring the emergence of collectivity and nucleon-nucleon interactions. Coulomb excitation of ^{136}Te on a titanium target was utilized to determine an extensive set of electromagnetic moments for the three lowest-lying states, including $B(E2; 0_1^+ \to 2_1^+)$, $Q(2_1^+)$, and $g(2_1^+)$. The results indicate that the first-excited state, 2_1^+, composed of the simple $2p \oplus 2n$ system, is prolate deformed, and its wave function is dominated by excited valence neutron configurations, but not to the extent previously suggested. It is demonstrated that extreme sensitivity of $g(2_1^+)$ to the proton and neutron contributions to the wave function provides unique insight into the nature of emerging collectivity, and $g(2_1^+)$ was used to differentiate among several state-of-the-art theoretical calculations. Our results are best described by the most recent shell model calculations.

DOI: 10.1103/PhysRevLett.118.092503

Atomic nuclei with two valence protons and two valence neutrons outside of double shell closures provide a simple and unique laboratory for exploring the emergence of collectivity and nucleon-nucleon interactions. Radioactive ^{136}Te, which possesses a robust ^{132}Sn core [1,2], is such an example. Previous measurements on neutron-rich Te isotopes around the $N = 82$ shell closure [3–7] have revealed both regular and irregular features in the electromagnetic moments with respect to empirical expectations and the nuclear shell model. In particular, an initial study of ^{136}Te [3] observed unexpectedly low electric quadrupole collectivity, i.e., $B(E2; 0_1^+ \to 2_1^+)$, with respect to ^{132,134}Te and shell-model calculations. The small $B(E2)$ value was attributed, in part, to a reduction in the pairing force. Furthermore, g-factor predictions [7–9], which are extremely sensitive to the wave function, yield discrepant values, indicating uncertainty on the underlying structure of this simple $2p \oplus 2n$ system. In this Letter, the collectivity of ^{136}Te is explored through the measurement of a complete set of electromagnetic moments, $B(E2; 0_1^+ \to 2_1^+)$, $Q(2_1^+)$, and $g(2_1^+)$.

A radioactive ion beam of ^{136}Te at an energy of 410 MeV was Coulomb excited on a 1.5 mg/cm^2 titanium target. The measurement was performed at the Holifield Radioactive Ion Beam Facility (HRIBF) of Oak Ridge National Laboratory (ORNL). The experimental setup included a HPGe Clover array, CLARION [10], a 2π CsI array, BareBall [11], and a Bragg-Curve gas detector. Electromagnetic moments were determined by measuring cross sections and particle-γ angular correlations of excited states following Coulomb excitation, cf. Refs. [7,12–16].

The self-supported titanium target was enriched and the isotopic composition was subsequently measured by inductively coupled plasma mass spectrometry (ICP-MS), resulting in 1.64(3)% ^{46}Ti, 1.35(3)% ^{47}Ti, 12.09(12)% ^{48}Ti, 3.52(4)% ^{49}Ti, and 81.40(81)% ^{50}Ti. The beam composition

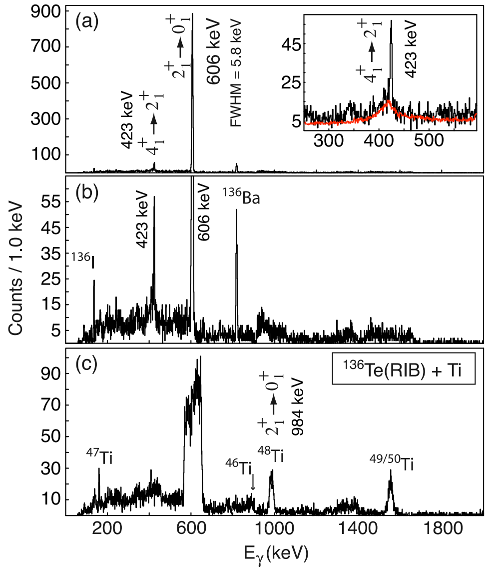

FIG. 1. The γ-ray spectra of (a) ^{136}Te, (b) ^{136}Te with a reduced vertical scale, and (c) $^{46–50}$Ti, using a different Doppler correction. The inset in panel (a) shows the $4_1^+ \to 2_1^+$ γ-ray transition and the Compton background. The Compton edge component (red) was modeled from data on ^{126}Te.

and energy loss through the target were directly measured with a zero-degree Bragg detector. The average beam composition was 3.9(6)% ^{136}Ba, 1.2(2)% ^{136}Cs, 9.3(14)% ^{136}I, and 85.6(15)% ^{136}Te. The energy loss of the beam through the target was determined to be 86(2) MeV from the Bragg detector and 83(2) MeV from the Doppler-shifted $2_1^+ \to 0_1^+$ transition of ^{136}Te, averaging to an adopted value of 84.5(14) MeV.

The Ti-gated γ-ray spectra are shown in Figs. 1(a)–1(c). The $2_1^+ \to 0_1^+$ (606 keV) and $4_1^+ \to 2_1^+$ (423 keV) transitions of ^{136}Te are clearly observed in Fig. 1(a). Unfortunately, the background under the $4_1^+ \to 2_1^+$ transition at 423 keV is obscured by the Compton edge of the $2_1^+ \to 0_1^+$ transition. The Compton background was modeled, cf. the inset in Fig. 1(a), from Coulomb-excitation data on ^{126}Te, which has a similar 2_1^+ energy but a different 4_1^+ energy. The $A = 136$ beam contaminants can be observed in Fig. 1(b). By changing the Doppler correction to the recoiling target nuclei, γ-ray transitions from the titanium isotopes can be observed, as shown in Fig. 1(c).

Coulomb-excitation cross sections and particle-γ angular correlations were measured at four different recoiling target angles using rings 1 through 4 of BareBall, covering $\theta_{\text{lab}} = 7°–60°$ or $\theta_{\text{cm}} = 166° - 60°$. A leading concern with using Coulomb excitation to extract accurate electromagnetic moments is the role of Coulomb-nuclear interference on the measured cross sections, which is destructive near the barrier [15,17,18]. Table I provides the effective $B(E2; 0_1^+ \to 2_1^+)$ values of ^{136}Te per BareBall ring for normalizations to Rutherford scattering and the $B(E2)$ of ^{48}Ti [19], assuming all other matrix elements are zero; the $4_1^+ \to 2_1^+$ yield of ^{136}Te has little to no impact on the $2_1^+ \to 0_1^+$ yield or effective $B(E2)$ value. Excellent consistency is found between the two normalizations for rings 2 and 3. The ^{48}Ti normalization for ring 1 is absent due to a lack of statistics. The Rutherford normalization for ring 4 is absent because the particle identification was not cleanly separated from the detector threshold due to the low energy of the recoiling target nuclei at the larger lab angles.

TABLE I. Effective $B(E2; 0_1^+ \to 2_1^+)$ e^2b^2 values of ^{136}Te per BareBall ring for normalizations to Rutherford scattering and the $B(E2)$ of ^{48}Ti, assuming all other matrix elements are zero. Only the statistical uncertainties are given.

Normalization	Ring 1	Ring 2	Ring 3	Ring 4
	$\theta_{\text{lab}} = 7–14°$	14-28°	28-44°	44-60°
	$\theta_{\text{cm}} = 166–152°$	152-124°	124-92°	92-60°
		Nominal		
Rutherford	0.137(10)	0.154(5)	0.158(4)	
^{48}Ti [a]		0.149(18)	0.155(12)	0.173(11)
		$V = 100$ MeV, $W = 0$ MeV		
Rutherford	0.139(10)	0.155(5)	0.159(4)	
^{48}Ti [a]		0.149(18)	0.155(12)	0.173(11)
		$V = 100$ MeV, $W = 40$ MeV		
Rutherford	0.142(10)	0.157(5)	0.159(4)	
^{48}Ti [a]		0.153(18)	0.156(12)	0.173(11)

[a] $B(E2; 0_1^+ \to 2_1^+) = 0.0662(29)$ e^2b^2 [19].

The effective $B(E2)$ values provided in Table I reveal a systematic decrease in magnitude with a decreasing ring number or an increasing center of mass angle. This destructive effect could be due to Coulomb-nuclear interference or reorientation from a prolate quadrupole deformation. The possibility of Coulomb-nuclear interference was investigated by performing calculations with the quantum code PTOLEMY [20] using two different optical potentials (V is the real potential and W is the imaginary or absorption potential). The results indicate that the Coulomb-nuclear interference effect is $< 3.6\%$ for ring 1; the effect is smaller for ring 2 and negligible for rings 3 and 4. Thus, the reorientation effect can be used to determine $Q(2_1^+)$.

Virtual excitations to higher-lying states were included in the analysis using the semiclassical Coulomb-excitation code GOSIA [21]. Details of the analysis procedures, including necessary corrections, can be found in Refs. [7,12–16]. The sensitivity or correlation between $\langle 0_1^+ || M(E2) || 2_1^+ \rangle = \sqrt{B(E2; 0_1^+ \to 2_1^+)}$ and $\langle 2_1^+ || M(E2) || 2_1^+ \rangle = 1.319 \times Q(2_1^+)$ per BareBall ring is shown in Fig. 2, revealing the presence of reorientation from a prolate quadrupole moment with a value of $Q(2_1^+) = -0.45(23)$ eb. The new $B(E2; 0_1^+ \to 2_1^+)$ value of 0.181(15) e^2b^2 is larger than the previous measurement of 0.122(18) e^2b^2 [3,4].

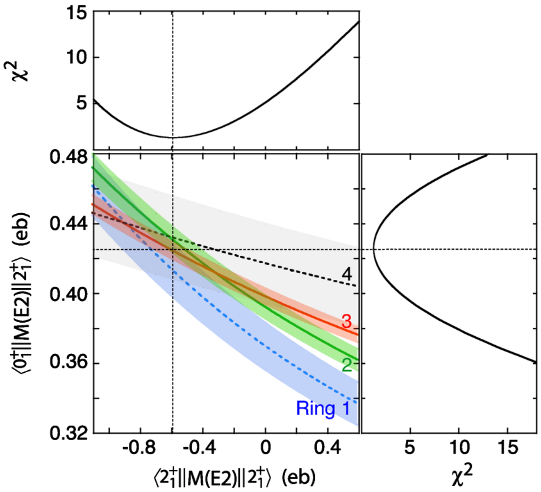

FIG. 2. Sensitivity of $\langle 0_1^+||M(E2)||2_1^+\rangle$ to $\langle 2_1^+||M(E2)||2_1^+\rangle$ per BareBall ring and the total χ^2.

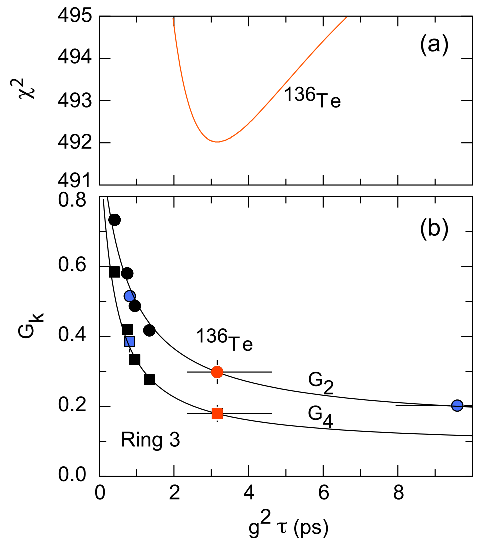

FIG. 3. (a) Total χ^2 vs $g^2\tau$ and (b) G_k vs $g^2\tau$ calibration curves for BareBall ring 3. The best fit $g^2\tau$ value for ^{136}Te, and its uncertainty, is projected onto the curves (red filled). Also shown are calibration data from stable Te isotopes that define the G_k curves [22]. Results for ^{125}Te are blue filled. Note that there is no G_4 term for $I = 3/2$ states and that the differences in G_k values for $I = 3/2, 2, 5/2$ are small compared to the experimental uncertainty.

The g factor was determined by the recoil in vacuum (RIV) method, following similar analysis procedures as for ^{124,126,128}Sn [13] and ^{132,134}Te [7,22] but with modification to accommodate the longer lifetime of the 2_1^+ state; previous studies focused on states with $\tau \lesssim 3$ ps, whereas here, the level of interest has $\tau \sim 30$ ps. Extensive RIV data were collected for ^{122,124,125,126,130}Te. These data will be reported in detail elsewhere [23]. The ^{125}Te data are particularly important here. The $3/2^+$, 444-keV state, with mean life $\tau = 27.6$ ps and g factor $g = +0.59(5)$ [24–26], allows calibration of the RIV interaction out to the necessary lifetime, while the $5/2^+$ 463-keV state in ^{125}Te, with $\tau = 19.0$ ps and $g = +0.207(22)$ [24–26], has nearly the same $g\tau$ value as the 2_1^+ state in ^{122}Te ($\tau = 10.8$ ps, $g = +0.353(14)$ [25]), but the two levels have very different g factors and lifetimes. In our earlier work on shorter-lived states, calibration curves of the vacuum attenuation coefficients G_k versus $|g|\tau$ were employed. It is evident from the ^{122,125}Te comparison, however, that G_k versus $g^2\tau$ is appropriate here. This altered dependence can be anticipated because atomic transitions during the nuclear lifetime become important for longer-lived states [22,27]. The G_k values were determined from fits to the angular correlations and calibration curves constructed, from which the g factor of ^{136}Te was then obtained. Figure 3 shows the calibration curves for BareBall ring 3 and the result of the fit to determine $g^2\tau$ for ^{136}Te. A g factor of $(+)0.34(^{+8}_{-6})$ is then obtained using $\tau = 27.5(23)$ ps from the present $B(E2)$ measurement. The sign $(+)$ is tentatively set by systematics and on the basis that no standard theory can predict a negative g factor of the observed magnitude.

The experimental electromagnetic moments for radioactive ^{136}Te are summarized in Table II and a comparison to several theoretical calculations, including the shell model (SM), Monte Carlo shell model (MCSM) [8], generator coordinate method with the Gaussian overlap approximation (GCM-GOA) [28], quasiparticle random phase approximation (QRPA) [9,29], alpha cluster (α) [30], and new shell model (NSM) [31], is provided. Interestingly, with only $2p \oplus 2n$ outside of double-magic ^{132}Sn, the experimental results and several of the theoretical calculations are consistent with rotational-like B_{42}/B_{20} ratios and $Q(2_1^+)$ values. Note that the $B_{20} \equiv B(E2; 2_1^+ \to 0_1^+) = B(E2; 0_1^+ \to 2_1^+)/5$ and $B_{42} \equiv B(E2; 4_1^+ \to 2_1^+)$ values in single-particle Weisskopf units are 8.71(74) and 14.4(22) W.u., respectively. Furthermore, the experimental magnitude of $g(2_1^+)$ is consistent with $0.8Z/A = 0.30$, which corresponds to the average empirical fraction of Z/A for heavy collective nuclei.

The present shell-model calculations (SM1 and SM2) included all proton single-particle orbits in the $Z = 50$–82 shell ($\pi 1g_{7/2}, 2d_{5/2}, 2d_{3/2}, 3s_{1/2}, 1h_{11/2}$) and all neutron orbits in $N = 82$–126 shell ($\nu 1h_{9/2}, 2f_{7/2}, 2f_{5/2}, 3p_{3/2}, 3p_{1/2}, 1i_{13/2}$). Single-particle energies were set by reference to ^{133}Sb and ^{133}Sn for protons and neutrons, respectively. The two calculations differ somewhat in the choice of interaction, effective charges, and effective $M1$ operator. Both, however, evaluated $E2$ matrix elements using standard harmonic oscillator radial wave functions, and both have been applied to ^{136}Te and neighboring nuclei in recent literature [32–35].

The SM1 calculation was performed with the NuShellX@MSU code [36]. As described in Refs. [32,33],

TABLE II. Summary of ^{136}Te electromagnetic moments, $B(E2)$ e^2b^2, Q eb, and g.

	Present Exp.	Exp. [3,4]	Present SM1	SM2	MCSM [8]	GCM-GOA [28]	QRPA [9]	QRPA2 [29]	α [30]	NSM [31]
$B(E2;0_1^+\to 2_1^+)$[a]	0.181(15)	0.122(18)	0.170	0.206	0.150	0.23	0.09	0.11	0.15	0.24
$B(E2;2_1^+\to 0_1^+)$	0.0362(31)	0.0244(36)	0.034	0.041	0.030	0.046	0.018	0.022	0.029	0.048
$B(E2;4_1^+\to 2_1^+)$	0.060(9)		0.048	0.052	0.033				0.040	0.068
$B(E2;2_2^+\to 0_1^+)$	<0.004		0.0002	0.003	0.006			0.015		0.0002
$B(E2;2_2^+\to 2_1^+)$	<0.09		0.023	0.040	0.001			0.002		0.030
$Q(2_1^+)$	−0.45(23)		−0.30	−0.26	−0.21	−0.37	−0.43			
$g(2_1^+)$	$(+)0.34(^{+8}_{-6})$		+0.34	+0.12	−0.11		−0.17			
B_{42}/B_{20}	1.66(34)		1.41	1.27	1.1				1.38	1.42

[a]$B(E2;0_1^+\to 2_1^+) = 5\times B(E2;2_1^+\to 0_1^+)$.

the interaction for the proton-proton space was based on the CD Bonn potential, and the proton-neutron and neutron-neutron interactions, designated $jj56pnb$, were obtained from the next-to-next-to-next-to-leading-order (N^{3}LO) potential. The effective charges were $e_p = 1.5e$ and $e_n = 0.5e$. Adjusting e_p and e_n to observed $E2$ transitions in ^{134}Te and ^{134}Sn, respectively, results in $e_p = 1.56e$ and $e_n = 0.66e$. These "optimized" effective charges increase the $B(E2)$ values by roughly 28% and the $Q(2_1^+)$ magnitude by 14%. However, the standard effective charges were adopted. The effective $M1$ operator applied a correction $\delta g_l(p) = 0.13$ to the proton orbital g factor and quenched the spin g factors for both protons and neutrons to 70% of their bare values. (The tensor term was ignored.) The effective $M1$ operator is then similar to that of Jakob *et al.* [37] and in reasonable agreement with that of Brown *et al.* [32]. For SM2, the two-body effective interaction was derived from the CD-Bonn NN potential, renormalized by means of the $V_{\text{low}-k}$ approach [38], within the framework of the perturbative $\hat{Q}$-box folded-diagram expansion [39]. In this case, $e_p = 1.7e$ and $e_n = 0.7e$, and the single-particle matrix elements of the effective $M1$ operator were calculated by perturbation theory, consistent with the derivation of the effective two-body interaction.

By comparing the various calculations in Table II and Fig. 4, the SM1 and SM2 shell-model calculations appear to best reproduce the experimental electromagnetic moments. All of the available $Q(2_1^+)$ predictions are consistent with the experimental value. However, while there is qualitative agreement amongst the predicted $E2$ transition strengths and $Q(2_1^+)$ values, there is a wide range of predictions for the $g(2_1^+)$ magnitude and sign; $g(2_1^+)$ is evidently very sensitive to the balance between proton and neutron contributions to the wave function. The larger g factor of SM1 relative to SM2 does not stem from the $M1$ operator because the value with the bare $M1$ operator in SM1 ($g = +0.23$) is larger than that in SM2 ($g = +0.02$). For both calculations, the decompositions of the wave functions indicate that the 2_1^+ wave function is dominated by excited valence neutron configurations. The leading component of the 2_1^+ wave function in SM1(SM2) is 40%(60%) $J_n = 2$, $J_p = 0$. The next leading term is 20% (16%) $J_n = 0$, $J_p = 2$, with all remaining terms <10%. Although SM1 has an increased proton content in better agreement with the experimental g factor, the wave function of the 2_1^+ state remains dominated by the neutron configuration. The leading components for the 4_1^+ and 2_2^+ states in SM1(SM2) are 32%(32%) $J_n = 4$, $J_p = 0$ and 42%(32%) $J_n = 2$, $J_p = 0$, respectively. With respect to the 2_2^+ state, the experimental limits on the $B(E2)$ values are inconsistent with recent predictions of a "mixed symmetry" state [8,9]. This leaves the 2_3^+ state as the better "mixed symmetry" candidate, as predicted by Covello *et al.* [40]; more experimental data are needed to clarify this point.

The $E(2_1^+)$, $B(E2;0_1^+\to 2_1^+)$, and $g(2_1^+)$ systematics for the radioactive Te isotopes around the $N = 82$ shell closure are provided in Fig. 5 and compared to the present SM1 and SM2 and previous MCSM [8] and QRPA [9] calculations. The SM1 and SM2 calculations for ^{132}Te used nucleon-nucleon interactions that were consistently derived within the procedure described above but for neutrons in the five orbits of the 50–82 shell. The SM1 and SM2 calculations consistently perform the best, particularly with respect to the g factor.

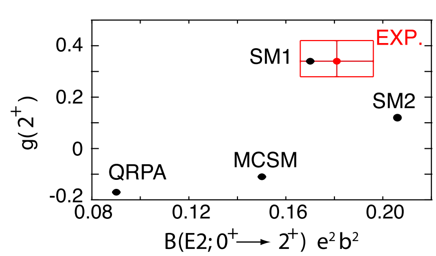

FIG. 4. The $g(2_1^+)$ versus $B(E2;0_1^+\to 2_1^+)$ experimental value (red), compared to the present SM1 and SM2 and previous MCSM [8] and QRPA [9] calculations.

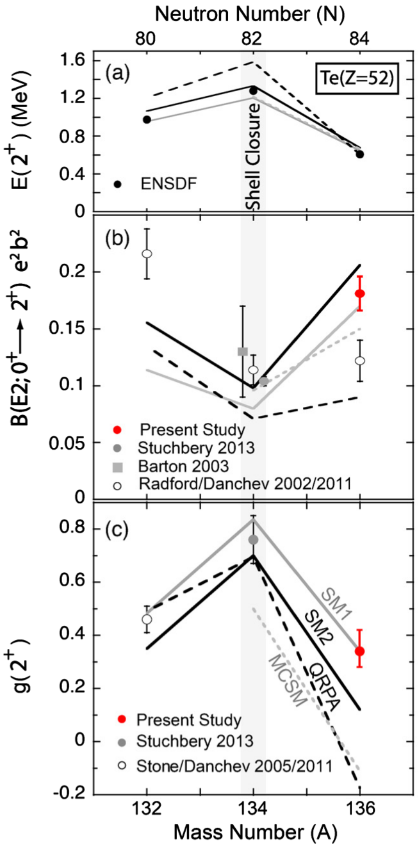

FIG. 5. The (a) $E(2_1^+)$, (b) $B(E2; 0_1^+ \to 2_1^+)$, and (c) $g(2_1^+)$ systematics for ^{132,134,136}Te from the present (red) and previous studies [3,4,6,7], compared to the present SM1 (solid gray line) and SM2 (solid black line) and previous MCSM (dashed gray line) [8] and QRPA (dashed black line) [9] calculations.

In conclusion, a complete set of electromagnetic moments, $B(E2; 0_1^+ \to 2_1^+)$, $Q(2_1^+)$, and $g(2_1^+)$, have been measured from Coulomb excitation of radioactive ^{136}Te, which has two protons and two neutrons outside of double-magic ^{132}Sn. Additionally, the value of $B(E2; 4_1^+ \to 2_1^+)$ and upper limits for $B(E2; 2_2^+ \to 2_1^+)$ and $B(E2; 2_2^+ \to 0_1^+)$ have also been determined. Present results for 2_1^+ indicate emergence of prolate-deformed quadrupole collectivity, and a greater proton content in its wave function than previously suggested. Further, these results are inconsistent with recent predictions of a 2_2^+ mixed-symmetry state, leaving the 2_3^+ state as the better candidate for this behavior. More importantly, it is demonstrated that extreme sensitivity of $g(2_1^+)$ to the proton and neutron contributions to the wave function provides unique insight into the nature of emerging collectivity, and may be utilized as a powerful tool to differentiate among various theoretical calculations. Our results are best described by the most recent state-of-the-art shell model calculations.

The authors gratefully acknowledge the HRIBF operations staff for providing the beams used in this study. This material is based upon work supported by the U.S. Department of Energy, Office of Science, Office of Nuclear Physics, under Contract No. DE-AC05-00OR22725, and this research used resources of the Holifield Radioactive Ion Beam Facility of Oak Ridge National Laboratory, which was a DOE Office of Science User Facility. This research was also sponsored by the Australian Research Council under Grant No. DP0773273, by the U.S. DOE under Contract No. DE-FG02-96ER40963 (UTK), and by the National Science Foundation, Grant No. PHY-1404442.

[1] K. L. Jones *et al.*, Nature (London) **465**, 454 (2010).
[2] J. M. Allmond *et al.*, Phys. Rev. Lett. **112**, 172701 (2014).
[3] D. C. Radford *et al.*, Phys. Rev. Lett. **88**, 222501 (2002).
[4] M. Danchev, G. Rainovski, N. Pietralla, A. Gargano, A. Covello, C. Baktash. J. R. Beene, C. R. Bingham, A. Galindo-Uribarri, K. A. Gladnishki, C. J. Gross, V. Y. Ponomarev, D. C. Radford, L. L. Riedinger, M. Scheck, A. E. Stuchbery, J. Wambach, C. H. Yu, and N. V. Zamfir, Phys. Rev. C **84**, 061306(R) (2011).
[5] C. J. Barton *et al.*, Phys. Lett. B **551**, 269 (2003).
[6] N. J. Stone, A. E. Stuchbery, M. Danchev, J. Pavan, C. L. Timlin, C. Baktash, C. Barton, J. R. Beene, N. Benczer-Koller, C. R. Bingham, J. Dupak, A. Galindo-Uribarri, C. J. Gross, G. Kumbartzki, D. C. Radford, J. R. Stone, and N. V. Zamfir, Phys. Rev. Lett. **94**, 192501 (2005).
[7] A. E. Stuchbery, J. M. Allmond, A. Galindo-Uribarri, E. Padilla-Rodal, D. C. Radford, N. J. Stone, J. C. Batchelder, J. R. Beene, N. Benczer-Koller, C. R. Bingham, M. E. Howard, G. J. Kumbartzki, J. F. Liang, B. Manning, D. W. Stracener, and C. H. Yu, Phys. Rev. C **88**, 051304(R) (2013).
[8] N. Shimizu, T. Otsuka, T. Mizusaki, and M. Honma, Phys. Rev. C **70**, 054313 (2004).
[9] J. Terasaki, J. Engel, W. Nazarewicz, and M. Stoitsov, Phys. Rev. C **66**, 054313 (2002).
[10] C. J. Gross *et al.*, Nucl. Instrum. Methods Phys. Res., Sect. A **450**, 12 (2000).
[11] A. Galindo-Uribarri, AIP Conf. Proc. **1271**, 180 (2010).
[12] J. M. Allmond, D. C. Radford, C. Baktash, J. C. Batchelder, A. Galindo-Uribarri, C. J. Gross, P. A. Hausladen, K. Lagergren, Y. Larochelle, E. Padilla-Rodal, and C. H. Yu, Phys. Rev. C **84**, 061303(R) (2011).
[13] J. M. Allmond, A. E. Stuchbery, D. C. Radford, A. Galindo-Uribarri, N. J. Stone, C. Baktash, J. C. Batchelder, C. R. Bingham, M. Danchev, C. J. Gross, P. A. Hausladen, K. Lagergren, Y. Larochelle, E. Padilla-Rodal, and C. H. Yu, Phys. Rev. C **87**, 054325 (2013).
[14] J. M. Allmond, B. A. Brown, A. E. Stuchbery, A. Galindo-Uribarri, E. Padilla-Rodal, D. C. Radford, J. C. Batchelder,

M. E. Howard, J. F. Liang, B. Manning, R. L. Varner, and C. H. Yu, Phys. Rev. C **90**, 034309 (2014).
[15] J. M. Allmond *et al.*, J. Phys. Conf. Ser. **639**, 012007 (2015).
[16] J. M. Allmond, A. E. Stuchbery, A. Galindo-Uribarri, E. Padilla-Rodal, D. C. Radford, J. C. Batchelder, C. R. Bingham, M. E. Howard, J. F. Liang, B. Manning, S. D. Pain, N. J. Stone, R. L. Varner, and C. H. Yu, Phys. Rev. C **92**, 041303(R) (2015).
[17] D. Cline, H. S. Gertzman, H. E. Gove, P. M. S. Lesser, and J. J. Schwartz, Nucl. Phys. **A133**, 445 (1969).
[18] P. M. S. Lesser, D. Cline, P. Goode, and R. Horoshko, Nucl. Phys. **A190**, 597 (1972).
[19] B. Pritychenko, M. Birch, B. Singh, and M. Horoi, At. Data Nucl. Data Tables **107**, 1 (2016).
[20] M. H. Macfarlane and S. C. Pieper, Argonne National Laboratory Report, Report No. ANL-76-11 1978 (unpublished).
[21] T. Czosnyka *et al.*, Bull. Am. Phys. Soc. **28**, 745 (1983).
[22] A. E. Stuchbery and N. J. Stone, Phys. Rev. C **76**, 034307 (2007).
[23] A. E. Stuchbery *et al.* (to be published).
[24] S. K. Chamoli, A. E. Stuchbery, and M. C. East, Phys. Rev. C **80**, 054301 (2009).
[25] A. E. Stuchbery, A.Nakamura, A, N. Wilson, P. M. Davidson, H. Watanabe, and A. I. Levon, Phys. Rev. C **76**, 034306 (2007).
[26] N. Benczer-Koller, G. Lenner, R. Tanczyn, A. Pakou, G. Kumbartzki, A. Piqué, D. Barker, D. Berdichevsky, and L. Zamick, Phys. Rev. C **40**, 77 (1989).
[27] X. Chen, D. G. Sarantites, W. Reviol, and J. Snyder, Phys. Rev. C **87**, 044305 (2013).
[28] G. F. Bertsch, M. Girod, S. Hilaire, J.-P. Delaroche, H. Goutte, and S. Péru, Phys. Rev. Lett. **99**, 032502 (2007).
[29] A. P. Severyukhin, N. N. Arsenyev, N. Pietralla, and V. Werner, Phys. Rev. C **90**, 011306(R) (2014).
[30] S. M. Wang, J. C. Pei, and F. R. Xu, Phys. Rev. C **87**, 014311 (2013).
[31] D. Bianco, N. Lo Iudice, F. Andreozzi, A. Porrino, and F. Knapp, Phys. Rev. C **88**, 024303 (2013).
[32] B. A. Brown, N. J. Stone, J. R. Stone, I. S. Towner, and M. Hjorth-Jensen, Phys. Rev. C **71**, 044317 (2005).
[33] J. M. Allmond *et al.*, Phys. Rev. C **90**, 014322 (2014).
[34] L. Coraggio, A. Covello, A. Gargano, and N. Itaco, Phys. Rev. C **88**, 041304(R) (2013), and references therein.
[35] L. Coraggio, A. Covello, A. Gargano, and N. Itaco, Phys. Rev. C **87**, 034309 (2013), and references therein.
[36] B. A. Brown, W. D. M. Rae, E. McDonald, and M. Horoi, NuShellX@MSU, http://people.nscl.msu.edu/~brown/resources/resources.html.
[37] G. Jakob, N. Benczer-Koller, G. Kumbartzki, J. Holden, T. J. Mertzimekis, K. H. Speidel, R. Ernst, A. E. Stuchbery, A. Pakou, P. Maier-Komor, A. Macchiavelli, M. McMahan, L. Phair, and L. Y. Lee, Phys. Rev. C **65**, 024316 (2002).
[38] S. Bogner, T. T. S. Kuo, L. Coraggio, A. Covello, and N. Itaco, Phys. Rev. C **65**, 051301(R) (2002).
[39] L. Coraggio, A. Covello, A. Gargano, N. Itaco, and T. T. S. Kuo, Prog. Part. Nucl. Phys. **62**, 135 (2009).
[40] A. Covello, L. Coraggio, A. Gargano, and N. Itaco, Prog. Part. Nucl. Phys. **59**, 401 (2007).